energies

MDPI

Article

Trombe Wall Thermal Behavior and Energy Efficiency of a Light Steel Frame Compartment: Experimental and Numerical Assessments

Victor Lohmann and Paulo Santos *

ISISE, Department of Civil Engineering, University of Coimbra, Pólo II, Rua Luís Reis Santos, 3030-788 Coimbra, Portugal; valohmann@gmail.com

* Correspondence: pfsantos@dec.uc.pt; Tel.: +351-239-797-199

Received: 29 April 2020; Accepted: 27 May 2020; Published: 30 May 2020

Abstract: Buildings are seeking renewable energy sources (e.g., solar) and passive devices, such as Trombe walls. However, the thermal performance of Trombe walls depends on many factors. In this work, the thermal behavior and energy efficiency of a Trombe wall in a lightweight steel frame compartment were evaluated, making use of in situ measurements and numerical simulations. Measurements were performed inside two real scale experimental identical cubic modules, exposed to natural exterior weather conditions. Simulations were made using validated advanced dynamic models. The winter Trombe wall benefits were evaluated regarding indoor air temperature increase and heating energy reduction. Moreover, a thermal behavior parametric study was performed. Several comparisons were made: (1) Sunny and cloudy winter week thermal behavior; (2) Office and residential space use heating energy; (3) Two heating set-points (20 °C and 18 °C); (4) Thickness of the Trombe wall air cavity; (5) Thickness of the thermal storage wall; (6) Dimensions of the interior upper/lower vents; (7) Material of the thermal storage wall. It was found that a Trombe wall device could significantly improve the thermal behavior and reduce heating energy consumption. However, if not well designed and controlled (e.g., to mitigate nocturnal heat losses), the Trombe wall thermal and energy benefits could be insignificant and even disadvantageous.

Keywords: passive solar; Trombe wall; light steel frame; thermal behavior; energy efficiency; Mediterranean climate; office use; residential use; heating set-points

1. Introduction

Energy is one of the main concerns when addressing sustainable development, especially since the world's energy matrix is still very dependent on fossil fuels, as oil and coal. The building's sector plays an important role, as buildings consume approximately 40% of the total energy in Europe, being also responsible for about 36% of the CO_2 emissions [1]. Aiming to improve the energy efficiency of buildings, the European Union (EU) has established the energy performance of buildings directive (EPBD) [2], in which two key concepts are defined: (1) the cost-optimal energy, regarding cost-efficiency of strategies [3], and (2) the nearly zero-energy buildings (nZEB)—buildings with very high energy efficiency—that cover their energy needs with energy produced by renewable sources, on-site or nearby [4]. To meet the EPBD requirements, the optimization of construction systems and the development of strategies to decrease energy consumption by buildings are key [5].

A sustainable strategy to improve the thermal and energy performance of buildings is exploiting solar energy, which also meets the EPDB establishments. A Trombe wall (TW) is a passive solar device that can be present in a building's façade to accumulate solar heat, heating, and even cooling indoor spaces, fostering natural ventilation [6]. This passive solar device was patented in 1881 by the

American engineer Edward Morse and popularized in the 1960s by the French engineer Felix Trombe and architect Jacque Michel, as mentioned by Saadatian et al. [7]. The classical configuration of Trombe walls is an outer glazed area to allow solar radiation to reach a massive storage wall, promoting the greenhouse effect. The storage wall usually has two interior vents (ventilated TW), connecting the indoor space to an air cavity between the wall and the glass panel—one at a lower height and other at an upper height [8]. To reduce heat losses through the TW device during cold winter nights, it is often used as an external night shutter [6]. Additionally, in warmer climates, exterior shading devices or overhangs are often used to mitigate overheating risk, as well as external upper and lower vents, promoting natural air-ventilation cooling effect during the summer season [9].

The operation of a Trombe wall is based on heat transfer principles. It absorbs solar heat in its high thermal mass storage wall during daytime and transfers part of this heat to the interior space of the building through conduction, radiation, and convection. The wall stores heat during the day and releases it during evening and night times, when the occupants require it and outdoor temperature decreases. The TW system, when exposed to direct solar radiation, exploits the greenhouse effect that occurs in the glazed air cavity, absorbing and storing heat in a massive wall. When the air cavity is warmed up by the heated storage wall, the air will flow upward due to buoyancy or thermosiphon effect. This heated air goes to the interior of the adjacent compartment through an upper vent, while colder air comes from the same room through a lower vent, re-entering to the TW air cavity [6].

Trombe walls have attracted attention over the last years, with different types studied, incorporating modern materials and construction methods, such as the incorporation of phase change materials [10] and photovoltaic cells on the glazed area [11].

Recently, Zhou et al. [12] studied the thermal performance of a composite Trombe wall under steady-state conditions. They compared three types of Trombe walls: traditional (TTW), water (WTW), and glass-water (GWTW). They optimized the thermal performance of the composite Trombe walls by defining two operating modes: (1) heat-collecting mode during the daytime, and (2) heat-preservation mode during night-time. The WTW exhibited the best efficiency during daytime (3.3% higher than the TTW) and also during night-time, allowing a heat loss reduction of 31% compared to TTW.

Besides space heating, researchers are also trying to develop new application advantages for Trombe walls. Hu et al. [13] made some experimental and numerical studies of a novel water blind-Trombe wall system. This new TW system, besides space heating and natural ventilation, could also provide domestic hot water since it made use of orientated steel blinds filled with flowing water and a hot water tank. They performed a comparison with conventional (i.e., without a glazing panel) and traditional TWs. A significant annual overall thermal load reduction was found compared to conventional (−42.6%) and traditional (−13%) Trombe walls. They also concluded that the new water blind-Trombe wall system, besides achieving a favorable insulation performance during winter, was also able to take advantage of the undesired solar radiation during the summer season to heat the water for domestic uses.

As mentioned before, Trombe walls could be very useful during the winter season to reduce space heating energy, but during the cooling season, this may have a negative impact due to limited control capability. Hong et al. [14] analyzed the thermal performance of a Trombe wall with an integrated Venetian blind during the cooling season. They evaluated the TW cooling mode operational control to regulate shading (from orientable Venetian blind slats within the TW air cavity) and natural ventilation (outside and cross). Several building occupation schedules were compared, i.e., service, office, and domestic buildings. It was found that the studied Venetian blind integrated TW could effectively prevent overheating through shading and ventilation. Moreover, they also concluded that the outside circulation mode was a more effective ventilation strategy to reduce cooling energy (5.0% to 5.8%) in comparison with the cross ventilation mode (2.5% to 4.6%).

Obviously, the thermal behavior and energy efficiency of buildings also depend on the buildings' envelope and construction system. In Tunisia, Abbassi et al. [15] performed numerical simulations, for a small single zone building (4 m × 4 m), to evaluate the heating energy savings provided by a

Trombe wall for different heavyweight building envelope façade walls (e.g., brick and stone), having different thermal transmittances (*U*-values), ranging from 2.035 W/(m^2·K) down to 0.388 W/(m^2·K) for a higher insulated exterior wall. For a smaller TW (3 m^2 area), they predicted heating energy savings, ranging from 28% up to 69%, for lower and higher thermal insulation levels, respectively. For a larger TW (6 m^2 area), the analogous heating energy savings ranged from 66% up to 98%.

An interesting alternative to traditional reinforced concrete and ceramic masonry construction is the lightweight steel frame (LSF) system, which has been attracting attention worldwide, given its functional, economic, and environmental advantages [16,17]. This lightweight innovative system presents construction flexibility and adaptability due to its modularity [18], safety at work, and construction economy due to the industrialized nature of the components, which also facilitates series production, prefabrication, and transportation [19]. In fact, several previous research studies have addressed the LSF system-related benefits, including sustainability [20], life cycle energy balance [21], and operational energy [22]. Nevertheless, an effort has been made to mitigate eventual drawbacks related to the thermal behavior of LSF construction, aiming to mitigate thermal bridges originated by the high thermal conductivity of the steel elements [23,24] and to increase the thermal inertia of this type of construction [25].

As mentioned before, the thermal behavior and energy efficiency of a Trombe wall depend on many factors, such as geometric (e.g., area, height, thickness, and orientation of the TW; existence and dimension of overhangs), materials' properties (e.g., storage wall thermal properties; glazed pane optical and thermal properties; shutter thermal properties; thermal insulation), fluid dynamics (e.g., dimensions and control of inner/outer and upper/lower vents; thickness of the air channel; natural or forced airflow), location (e.g., latitude; north or south hemisphere), and weather (e.g., solar radiation level and incidence angle; nocturnal cloudy or clear sky; temperature; wind speed, and direction) [6]. Thus, it is not an easy task to adequately design and control a TW device to take full thermal, energy, and economic advantages [26,27].

As stated before, despite the LSF system advantages, there are also possible drawbacks, such as the reduced thermal inertia, due to its natural weightlessness, compared to traditional concrete structures [28]. Thus, it would be interesting to evaluate the effect of a solar passive Trombe wall device, which is characterized by having a massive storage wall, on an LSF construction system, having low thermal inertia and reduced mass. However, this kind of research has not been found in the literature. Moreover, research works on water Trombe walls are very scarce. Therefore, in this work, the influence of a passive solar water Trombe wall (TW) device on the thermal behavior and energy efficiency of a lightweight steel frame (LSF) compartment, located in Coimbra (Portugal), was studied, being this evaluation based in numerical simulations and in situ measurements. Measurements of indoor air temperature were performed inside two real scale experimental identical cubic modules, exposed to natural exterior weather conditions, while simulations were performed using advanced dynamic models, validated experimentally.

First, the experimental approach has been described, regarding the LSF experimental modules, the TW prototype, the weather stations, and temperature/humidity data-logger sensors. After, the numerical approach has been detailed, including the 2D thermal computations to obtain the *U*-values of the LSF components and the advanced numerical simulations. Next, the calibration and model validation has been reported for both reference and TW LSF models, and some computational fluid dynamics (CFD) results have also been reported. Afterward, the obtained results have been discussed and grouped in TW benefits and parametric study. The winter TW benefits were evaluated regarding indoor air temperature increase and heating energy reduction. The thermal behavior parametric study was performed for several TW key-factors, such as the thicknesses of the air cavity and storage wall and dimensions of the internal vents and the storage wall materials. Finally, some concluding remarks about this research work have been highlighted.

2. Materials and Methods

The materials and methods used in this research have been described in detail in this section, starting with the experimental and numerical approaches, followed by the calibration and validation of the advanced dynamic thermal simulation models of the LSF modules and water Trombe wall.

2.1. Experimental Approach

2.1.1. LSF Experimental Modules

The experimental measurements were performed on two similar lightweight steel frame (LSF) modules constructed near the Department of Civil Engineering (DEC) of the University of Coimbra (Portugal), as illustrated in Figure 1, having a GPS coordinates: 40.1855° N, 8.4167° W. Those experimental modules were two identical cubic compartments constructed in LSF, with inner dimensions: (L) 2.75 m × (W) 2.75 m × (H) 2.80 m. Module 1 was used as a reference (for results comparison), while module 2 had a water Trombe wall prototype on its south facade.

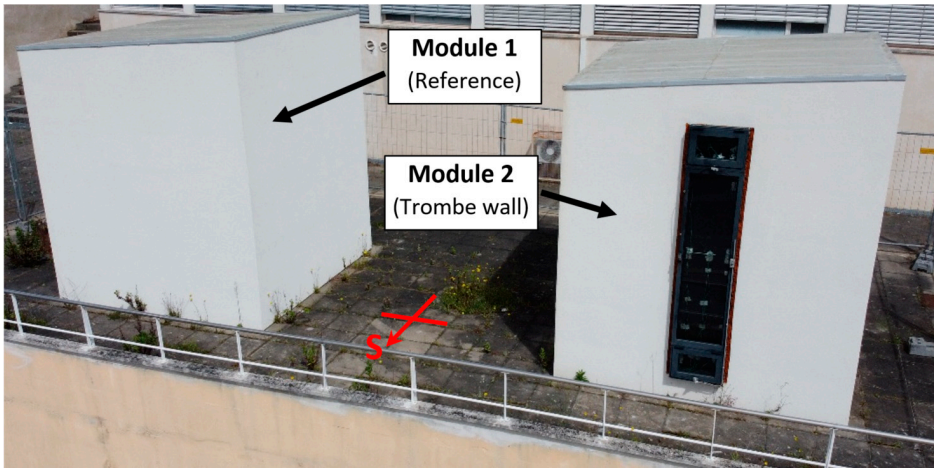

Figure 1. LSF (lightweight steel frame) experimental modules constructed at the University of Coimbra, Engineering Campus (GPS: 40.1855° N, 8.4167° W).

The external dimensions of the experimental modules, as well as the material specifications of the LSF construction elements, such as the number of layers, materials, and thicknesses, are schematically illustrated in Figure 2, while Table 1 displays the thermal conductivities of the materials. In these experimental modules, the LSF system B(A)[a] was adopted and manufactured by Urbimagem company [29], making use of steel profiles C100 × 45 × 1.5 mm. The structural sheathing was provided by 12 mm oriented strand board (OSB) panels [30] on both sides of the walls' steel frame. The ceiling was also inferiorly lined with OSB panels, as well as the upper side of the roof steel frame beams. To allow access to the interior, both modules had a similar wooden door (2.00 m high by 0.78 m wide), which was thermally insulated with the same expanded polystyrene (EPS) external thermal insulation composite system (ETICS) system of the walls. There were no windows in the experimental TW modules. This was justified by the intention to isolate the TW effect in the evaluated compartments. A glazed window (e.g., south orientated) would provide additional solar heat gains, which would be overlapped and more difficult to distinguish from the heat gains provided by the TW device.

Notice that, as illustrated in Figure 2, the experimental modules were designed to have gypsum plasterboard (GPB) as an inner sheathing layer of walls and ceiling, but later it was decided not to apply these GPB panels. The batt insulation was provided by 100 mm mineral wool (MW) [31], fulfilling the air-cavity between the steel frame. The exterior thermal insulation composite system (ETICS) was made with EPS thermal insulation [32] (50 mm thick) and finished by a reinforced plaster layer (5 mm). The exterior thermal insulation of the roof was made of extruded polystyrene (XPS) [33] with the same

thickness. To avoid moisture direct contact from the ground, the floor was 300 mm elevated, creating a small crawl space below, as illustrated in Figure 2, having an 18 mm OSB panel [30] below and another above the continuous XPS [34] thermal insulation layer (60 mm thick). The inclined flat roof was waterproofed by a polyvinyl chloride (PVC) membrane [35] (1.5 mm thick), forming a plenum above the ceiling with variable thickness.

Table 1. Thermal conductivity (λ) of the materials used in the lightweight steel frame (LSF) modules.

Materials		λ ((m·K)/W)	Reference
Reinforced plaster (ETICS [1] finish)		0.720	[37]
EPS [2] (ETICS [1] thermal insulation)		0.036	[32]
OSB [3] (LSF sheathing)		0.130	[30]
Mineral wool (cavity insulation)		0.037	[31]
Steel (profiles C100 × 45 × 1.5 mm)		50.000	[38]
XPS [4]	(roof insulation)	0.036	[33]
	(floor insulation)	0.035	[34]
Vinyl floor cover		0.250	[39]
PVC [5] membrane (roof waterproofing)		0.170	[35]
Wooden door		0.144	[40]

[1] ETICS, external thermal insulation composite system; [2] EPS, expanded polystyrene; [3] OSB, oriented strand board; [4] XPS, extruded polystyrene; [5] PVC, polyvinyl chloride.

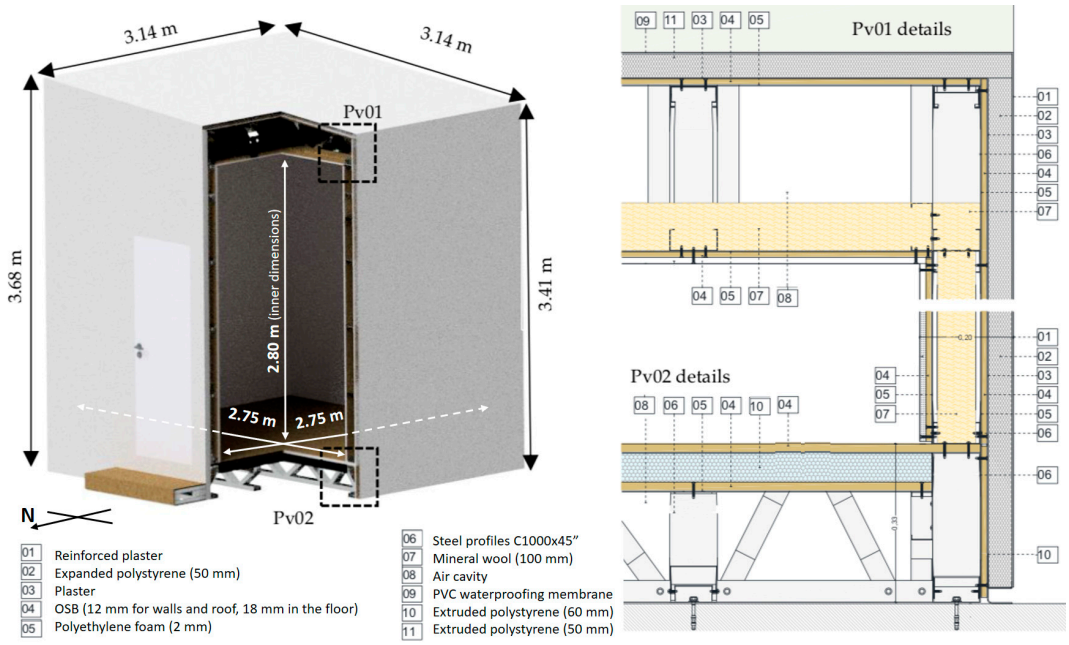

Figure 2. Schematic details of the LSF modules construction elements (adapted from [36]).

Table 2 displays, for each LSF element, the materials and thicknesses of the layers, as well as the computed thermal transmittance (*U*-value). Notice that two types of layers were assessed in these LSF elements: (1) homogeneous, where the steel frame was not included in the thermal computations, given its location outside the insulation and sheathing materials, and (2) inhomogeneous, where the steel frame crossed through the insulation materials (e.g., mineral wool). The *U*-value for the elements with homogeneous layers (floor, roof, and door) was computed following the analytical calculation procedures prescribed by standard ISO 6946 [41]. The *U*-values of the LSF elements

containing inhomogeneous layers (walls and ceiling) were computed, making use of bi-dimensional (2D) finite element method (FEM) models built in the THERM software [42], as has been detailed next in Section 2.2.1. The obtained *U*-values (Table 2) ranged from 0.326 W/(m^2·K) in the walls up to 0.670 W/(m^2·K) in the ceiling.

Table 2. Materials, thicknesses (*d*), and thermal transmittances (*U*) of the LSF elements.

Element (Layers Type)	Materials (Layers from Outer to Inner Surfaces)	*d* (mm)	*U*-Value (W/(m^2·K))
Walls (inhomogeneous)	Reinforced plaster (ETICS [1] finish)	5	0.326
	EPS [2] (ETICS [1] thermal insulation)	50	
	OSB [3] (LSF sheathing)	12	
	Mineral wool (cavity insulation)	100	
	OSB [3] (LSF sheathing)	12	
	Total thickness =	179	
Floor (homogeneous)	OSB [3] (LSF sheathing)	18	0.426
	XPS [4] (floor slab insulation)	60	
	OSB [3] (LSF sheathing)	18	
	Vinyl floor cover	3.4	
	Total thickness =	99.4	
Ceiling (inhomogeneous)	Mineral wool (cavity insulation)	100	0.670
	OSB [3] (LSF sheathing)	12	
	Total thickness =	112	
Roof (homogeneous)	PVC [5] membrane (roof waterproofing)	1.5	0.613
	XPS [4] (exterior thermal insulation)	50	
	OSB [3] (LSF sheathing)	12	
	Total thickness =	63.5	
Door (homogeneous)	Reinforced plaster (ETICS [1] finish)	5	0.534
	EPS [2] (ETICS [1] thermal insulation)	50	
	Wooden door	44	
	Total thickness =	99	

[1] ETICS, external thermal insulation composite system; [2] EPS, expanded polystyrene; [3] OSB, oriented strand board; [4] XPS, extruded polystyrene; [5] PVC, polyvinyl chloride.

2.1.2. Trombe Wall Prototype

The Trombe wall prototype (2.80 m high and 0.55 m wide) was placed on the south-oriented wall of module 2 (Figure 1). Figure 3a schematically illustrates the geometry of this Trombe wall prototype, which was developed and executed during a Ph.D. research work [36]. Notice that the dimensions of this modular TW prototype were defined, taking into account the ceiling height (2.80 m) and the usual vertical steel stud spacing in LSF construction (0.60 m). The thermal storage wall was made with a black-painted steel sheet tank fulfilled with water, having 50 mm of thickness. On the outer side, there was an aluminum frame glazing system with double glass (4 mm + 16 mm of argon + planistar 6 mm), having an effective solar absorption area of 1.1 m^2. The glazing panel had a solar heat gain coefficient (SHGC) equal to 0.743, while the direct solar transmission was 0.667, and the thermal transmittance was 2.552 W/(m^2·K), as displayed in Figure 3b.

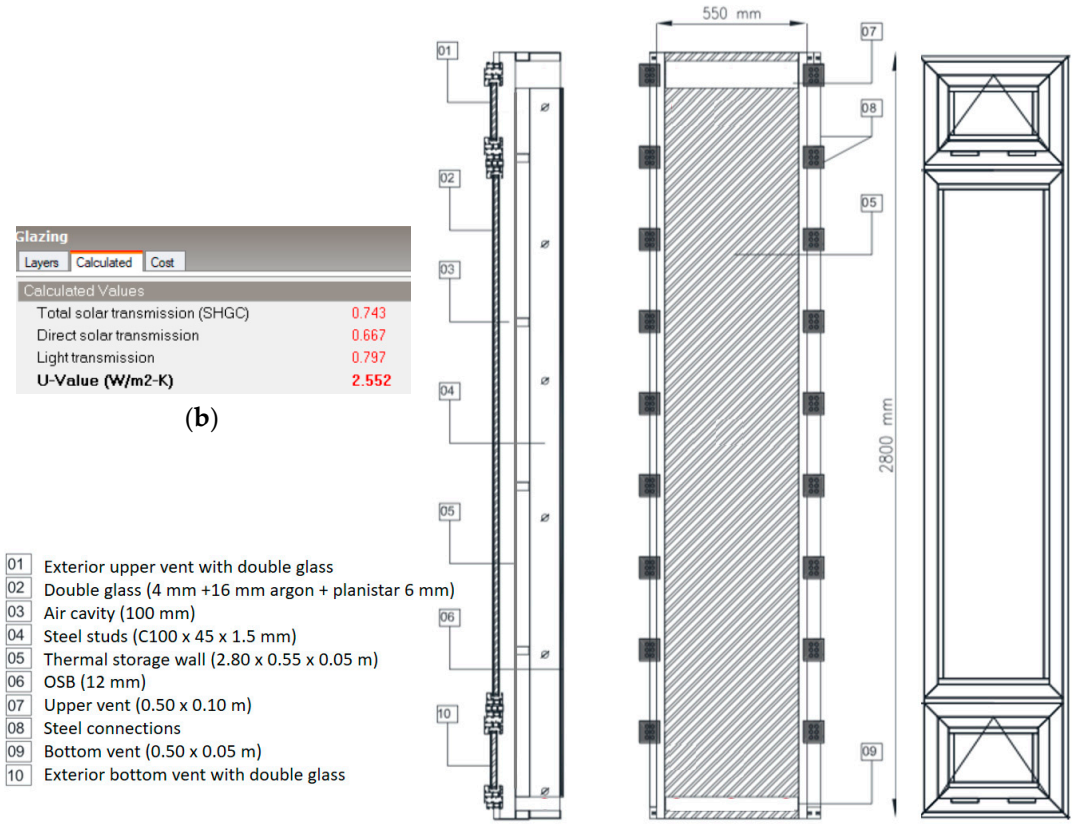

Figure 3. Trombe wall prototype: (**a**) Schematic geometry details (adapted from [36]); (**b**) Glazing optical and thermal properties.

This glazed aluminum frame had a top and lower exterior openings for exterior ventilation, which were not used during these experiments, being all the time closed. Between the storage wall and the outer glazing, there was a 100 mm thick air cavity. On the inner surface of the storage wall, there was a layer of 0.10 m of mineral wool, covered by an OSB panel (12 mm). To allow air circulation between the outer air cavity and the indoor environment, there were two rectangular air vents on the Trombe wall: (1) an upper air vent, 0.50 m wide by 0.10 m high, and (2) a bottom air vent with the same width but a smaller height (0.05 m).

2.1.3. Monitoring Equipment

To reproduce the thermal behavior of the experimental modules exposed to exterior weather conditions, it was needed to have access to hourly weather data recorded nearby. With this purpose, two weather stations were used: (1) Department of Mechanical Engineering (DEM) [43], also located in the Engineering campus of the University of Coimbra (GPS: 40.1849° N, 8.4132° W), and (2) CoolHaven company [44], located in Coimbra iParque, Antanhol (GPS: 40.1792° N, 8.4654° W).

The nearest weather data station (DEM) was used for most of the data needed to perform advanced dynamic simulations, including air temperature, dew-point temperature, relative humidity, wind direction, wind speed, atmospheric pressure, and precipitation. However, this weather station did not provide some additional relevant weather data, such as the parameters related to solar radiation, i.e., global horizontal radiation, diffuse horizontal radiation, and direct normal radiation. This essential detailed solar radiation information was obtained in the CoolHaven weather station, located about 7 km from the experimental modules.

Regarding the hardware, the DEM weather station is a wireless Davis Vantage Pro2 Plus [45], while the CoolHaven is constituted of several sensors, with the pyranometer being a sunshine sensor Delta-T BF5 [46].

Notice that according to the Köppen–Geiger climate classification [47], the city of Coimbra (Portugal) is located in a Csb climate region, which is characterized by a temperate climate with rainy winter and dry summer slightly hot, being a very frequent climate within the Mediterranean region [16].

The indoor air temperature and humidity were measured simultaneously, inside both LSF modules, to monitor their thermal behavior and verify the influence of the solar Trombe wall. With this purpose, one Tinytag Ultra 2—TGU-4500 [48] air temperature and humidity sensor was installed inside each module, being suspended in the middle ceiling, at mid-height. These sensors were factory calibrated, having a precision of ±0.45 °C for temperature and ±3% for relative humidity. The measured data was averaged and recorded every 10 minutes, having a sampling interval of 10 seconds. The in situ measurements took place from the 26th of July 2019 until the 19th of January 2020.

2.2. Numerical Approach

2.2.1. 2D FEM Thermal Computations

As mentioned before (see Section 2.1.1), the *U*-values of the inhomogeneous LSF elements (walls and ceiling) were computed, making use of bi-dimensional (2D) models implemented in a finite element method (FEM) software: THERM [42]. The FEM mesh was refined to have a maximum error of 2%.

LSF Ceiling Element

For the ceiling element, as the steel profiles are placed only in one direction (see the yellow region in Figure 4a), the *U*-value was directly obtained from the 2D FEM model, as illustrated in Figure 4b. The model had a width of 600 mm, i.e., equal to the distance between the steel studs within the ceiling. The steel C stud was positioned in the middle of the model, as shown in Figure 4b, and this is a representative part of the LSF ceiling slab. Moreover, the ceiling mineral wool (MW) insulation was considered only between steel sections since, in practice, it was not possible to put MW inside the corresponding steel lattice beam, where it was considered an air gap. Figure 4c displays the temperature distribution predicted in the ceiling cross-section, where the thermal bridged effect was clear due to the MW thermal insulation discontinuity. The global *U*-value computed from the THERM model was 0.670 W/(m^2·K). Notice that assuming homogeneous layers, i.e., considering continuous MW insulation and neglecting the steel studs, the *U*-value obtained was 0.334 W/(m^2·K), being 50% smaller.

LSF Wall Element

Since the LSF walls had steel studs in vertical, horizontal, and diagonal planes (see Figure 5a), the bi-dimensional *U*-value computation procedure was different from the ceiling element, where the *U*-value was directly obtained from the THERM model. It is well known that an insulated LSF element has two distinct thermal zones [49,50]: (1) an increased heat transfer zone (lower thermal resistance) in the vicinity of the steel studs, given the high thermal conductivity of steel, and (2) a more reduced heat transfer zone (higher thermal resistance) in the insulated cavity between the steel studs. Thus, the global thermal transmittance (U_{global}) of LSF elements with complex steel frame could be estimated, making an area-weighted summation of the *U*-values for each thermal zone mentioned before ("stud" and "cav"), as given in the following equation:

$$U_{global} = \frac{U_{\text{stud}}.A_{\text{stud}} + U_{\text{cav}}.A_{\text{cav}}}{A_{\text{global}}} \quad (1)$$

where A_{global} is the total area of the LSF element (internal dimensions), A_{stud} is the total area of influence of the steel stud on the LSF element, and A_{cav} is the remaining cavity area of the LSF wall. For this specific LSF wall, the areas considered in the computations are displayed in Figure 5a.

Both U-values (U_{stud} and U_{cav}) were obtained, making use of a THERM model, as illustrated in Figure 5b. This simplified LSF wall model had a length equal to the spacing between the vertical steel studs, i.e., 600 mm. To obtain the two representative U-values, two "measurement" zones were simulated in the LSF wall model: one right under the steel stud and another one in the edge of the wall cavity. These "measurement" zones were modeled having the same width as the steel stud flange, i.e., 45 mm, and is delimited in Figure 5 by two dashed white lines.

Figure 5c displays the obtained temperature (°C) color distribution along the cross-section of the LSF wall model and is well visible in the thermal bridge originated by the central steel stud and its correspondent temperature disturbance. Figure 5d shows the computed heat flux (W/m^2) distribution within the cross-section of the LSF wall, as well as the two U-values computed in the steel stud vicinity and in the edge of the wall cavity. As expected, the U_{stud} (0.797 W/m^2·K) was considerably higher (+260%) than the U_{cav} (0.221 W/m^2·K), confirming the huge relevance of the steel stud (only 1.5 mm thick) in the thermal performance of the LSF wall.

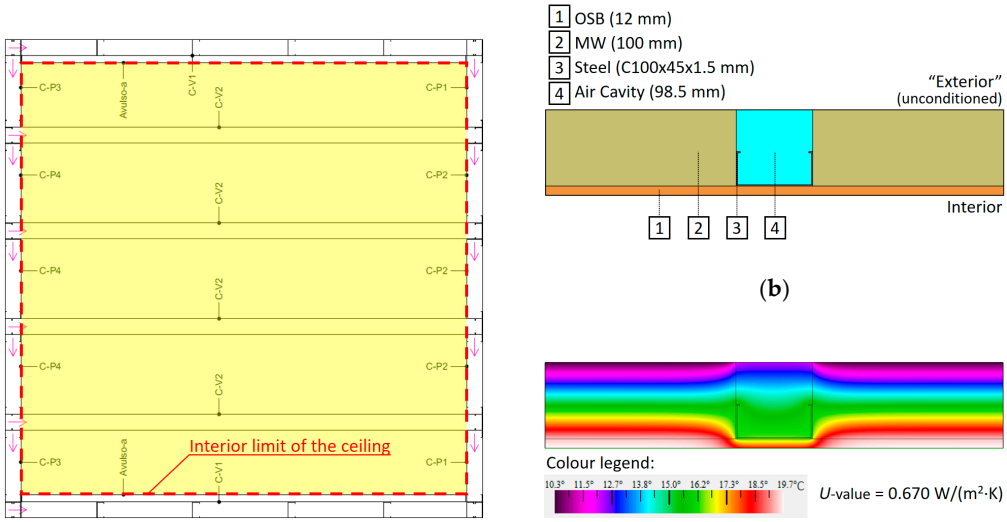

Figure 4. LSF ceiling element: (**a**) Plan view of the ceiling steel frame; (**b**) THERM model; (**c**) Temperature color distribution and obtained U-value.

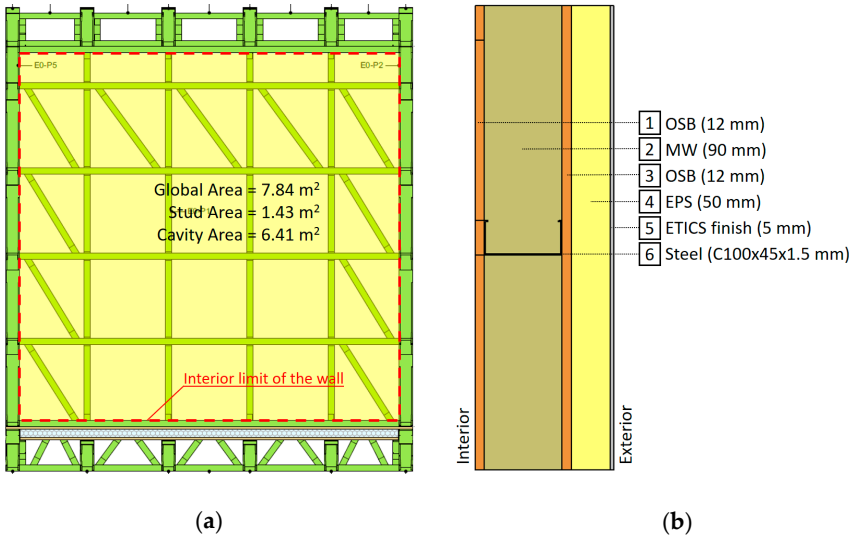

Figure 5. *Cont.*

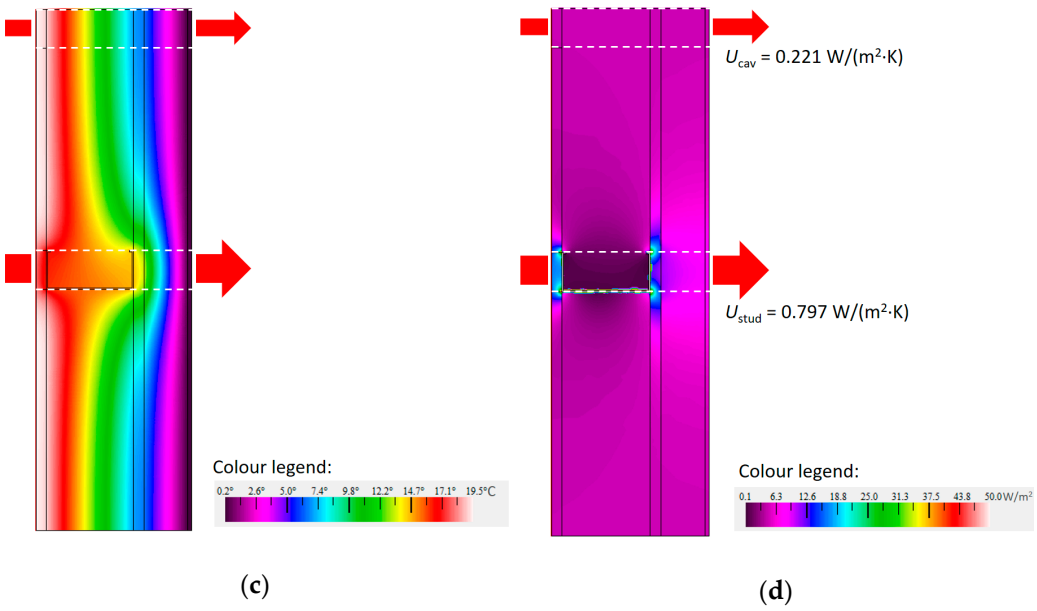

Figure 5. LSF wall element: (**a**) Frontal view of the wall steel frame; (**b**) THERM model; (**c**) Temperature color distribution; (**d**) Heat flux distribution and local *U*-values.

Finally, knowing the three areas (Figure 5a) and the two *U*-values (Figure 5d) and making use of Equation (1), a global *U*-value equal to 0.326 W/(m^2·K) was obtained. Notice that when the steel studs were neglected and homogenous layers were assumed, the *U*-value reduced to 0.225 W/(m^2·K) (31% smaller).

It is important to highlight that there are several strategies to mitigate the thermal bridges originated by steel studs within an LSF component, reducing their *U*-value, such as the use of thermal break (TB) strips within steel studs flange [51]. These TB strips could be made of different materials, such as recycled tire rubber [52]. Shortly, it was intended to use this type of TB strips to improve the thermal performance of these experimental LSF modules.

2.2.2. Advanced Dynamic Simulations

The advanced dynamic thermal simulations were performed in the software DesignBuilder version 5.5.0.012 (DesignBuilder Software Ltd, Stroud, Gloucester, UK) [37]. The computations were performed, making use of hourly interval data. A replica of the two LSF experimental modules photographed in Figure 1 was modeled, taking into account the location/climate, the geometry/dimensions, the construction elements composition (e.g., walls, floor, ceiling, roof, door, and Trombe wall), the material properties, the airtightness, the activity, and occupation parameters. Figure 6 exhibits a print-screen view of the two models: (1) module 1, used as reference (Figure 6a), and (2) module 2, containing the Trombe wall (Figure 6b).

The airtightness of these experimental modules was measured in-situ [36], and the obtained value (0.05 air changes per hour) was implemented in the DesignBuilder model as a constant value and without any natural ventilation since, during the measurements, the openings (back door and Trombe wall exterior vents) were always closed. Moreover, the modules were kept empty, i.e., without anyone inside. Thus, the occupancy was set as "null", and the activity tab as "none". Notice that the color of the materials was also reproduced, in particular, the black color of the Trombe wall (Figure 6b).

2.3. Calibration and Model Validation

To ensure good reliability of the DesignBuilder [37] advanced dynamic models (Figure 6) thermal behavior predictions, the obtained simulation results were compared with the air temperature in-situ measurements (see Section 2.1.3), performed inside the LSF modules (Figure 1), subjected to natural

outdoor weather conditions (recorded nearby, as previously explained in Section 2.1.3), allowing to validate these models, as shown next.

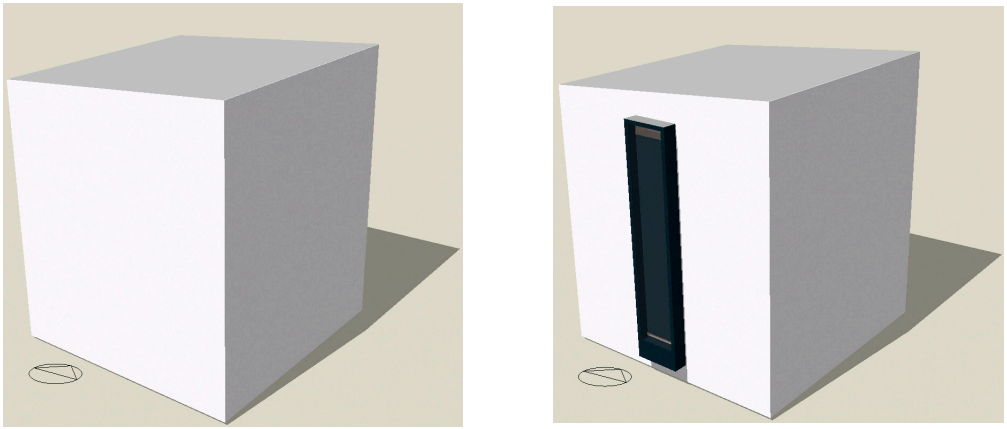

Figure 6. DesignBuilder models southeast views: (**a**) Module 1 (Reference); (**b**) Module 2 (Trombe wall, TW).

2.3.1. Reference LSF Model

Figure 7 presents a graph with a comparison among predicted and measured indoor air temperatures in the reference LSF module (module 1) during one week (2–8 September 2019). A good agreement between the DesignBuilder model predictions and the in-situ indoor air temperatures was observed. In fact, both average temperatures were very similar: 26.4 °C (recorded) and 26.3 °C (predicted). Moreover, the root mean square error (RMSE) was only 0.3 °C, allowing to conclude that this DesignBuilder advanced dynamic simulation reference LSF model was calibrated and experimentally validated.

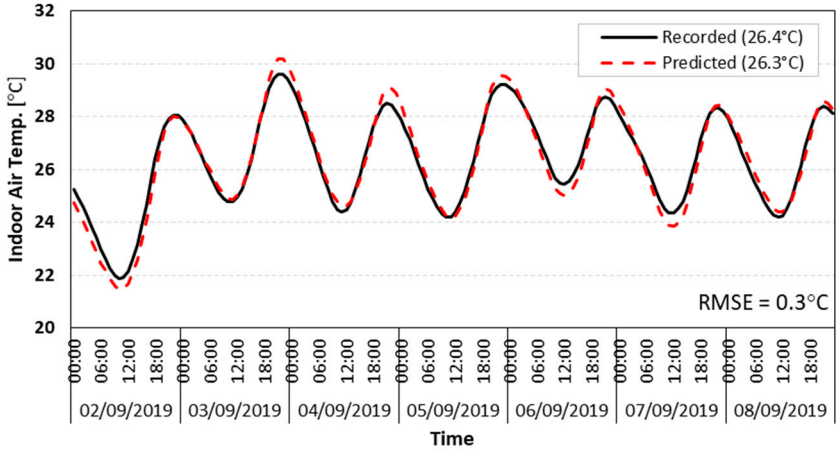

Figure 7. Predicted and measured indoor temperatures in module 1 (reference).

2.3.2. Trombe Wall LSF Model

The accuracy of the Trombe wall LSF model was also verified by comparison among predicted and measured indoor air temperatures. Figure 8 displays the obtained results plot, in which a good agreement between both curves was observed. The RMSE for this model was 0.5 °C, confirming also a good accuracy performance of this second model.

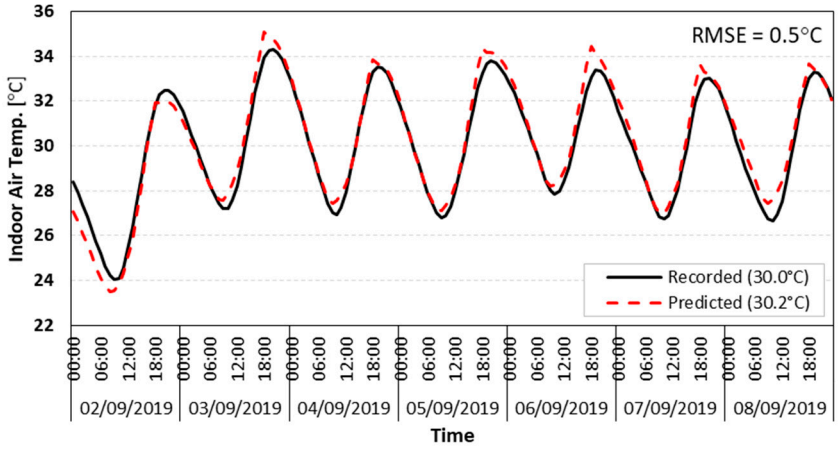

Figure 8. Predicted and measured indoor temperatures in module 2 (with a Trombe wall).

2.3.3. Trombe Wall CFD Assessment

To verify if the modeled Trombe wall is operating coherently, a computational fluid dynamics (CFD) analysis was also conducted on DesignBuilder, which has a built-in CFD tool. Figure 9 displays the results of the CFD analysis, carried for the 16:00 hours of the 4th of September, with both air velocity and temperature in a color scale being displayed, as well as velocity vectors.

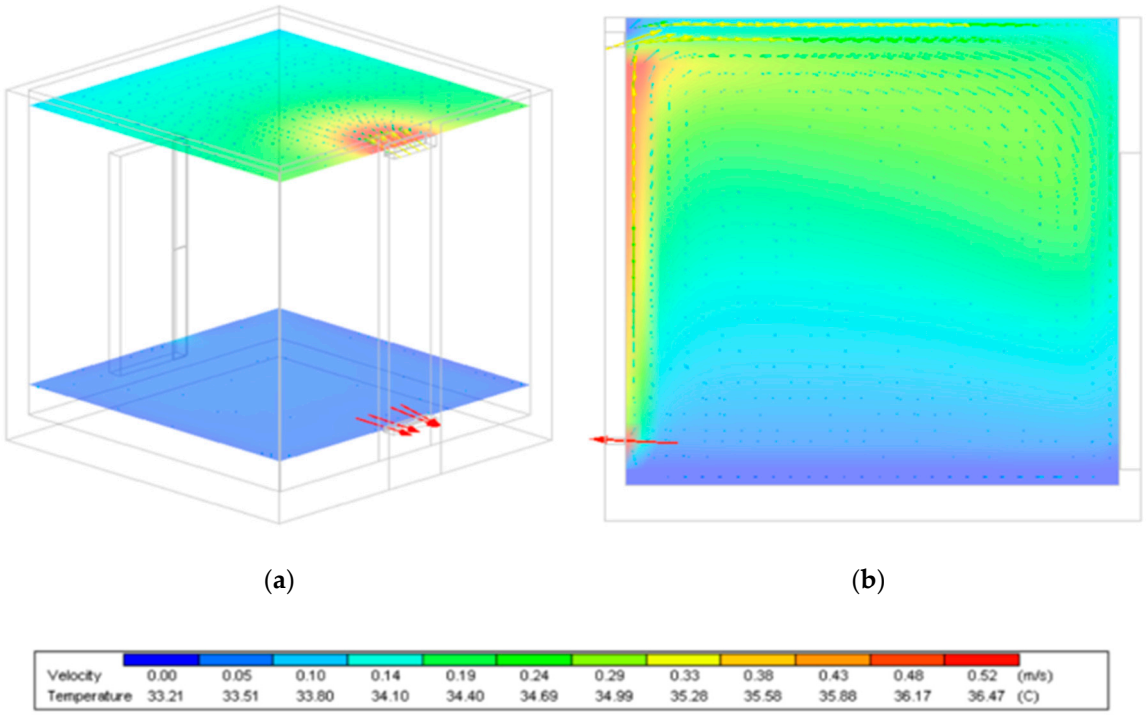

Figure 9. CFD (computational fluid dynamics) analysis (air velocity and temperature) of module 2 (with a Trombe wall): (**a**) Horizontal planes at vent levels; (**b**) Vertical plane in front of the Trombe wall.

Looking at the results of the horizontal plane plotted in Figure 9a was well visible the colder air entrance to the Trombe wall air cavity through its lower vent, as well as the warmer air flowing out of the upper vent near the ceiling. Moreover, in Figure 9b (the vertical plane in front of the Trombe wall), the air stratification in height and also the air being heated near the Trombe wall were again visible, which was exposed to direct solar radiation (4 pm) and, consequently, was flowing up to the ceiling. Therefore, these CFD simulation results made sense and were coherent with the expected ones for a

compartment with a Trombe wall exposed to direct solar radiation, which ensured the reliability of the implemented models.

3. Results and Discussion

In this section, the obtained results have been presented and discussed, starting with the Trombe wall benefits, regarding the thermal behavior and heating energy savings. Thereafter, the results of the sensibility analysis, for several Trombe wall parameters, have been described and discussed.

3.1. Trombe Wall Benefits

In this section, the water Trombe wall benefits were assessed, making use of in situ indoor air temperature measurements (Section 3.1.1.) and advanced dynamic numerical simulations for the heating energy reduction predictions (Section 3.1.2.). These assessments were performed by comparison between module 1 (the reference one) and module 2 (the one with a Trombe wall) located in the city of Coimbra (Portugal), during winter.

3.1.1. Indoor Temperature Increase

The indoor air temperature comparisons were made using the data from measurements taken simultaneously with the temperature and humidity sensors [48], on both modules (with and without the Trombe wall) and are plotted in Figure 10, as well as the exterior environment air temperature. Two distinct winter weeks were chosen to demonstrate the behavior of the modules under different weather conditions. In Figure 10a, the records for a sunny week (from 28th of December to 3rd of January) are displayed, while in Figure 10b, the measurements for a cloudy week (from 16th to 22nd of December) are shown.

In the sunny winter week (Figure 10a), the indoor air temperature increase in module 2 due to the Trombe wall was well visible, having an average temperature of 16.2 °C, i.e., a temperature increase of 3.3 °C relative to module 1. Notice that even with a Trombe wall, the indoor comfort air temperature (e.g., 18 °C) was not reached. Another interesting feature was that the daily indoor air temperature amplitude (or fluctuation) was also greater in the experimental module with the Trombe wall (module 2), having a higher temperature increase rate during the day (due to the solar heat gains) and also a higher temperature decrease rate during the night (due to the higher heat losses through the Trombe wall, which did have any night shutter device).

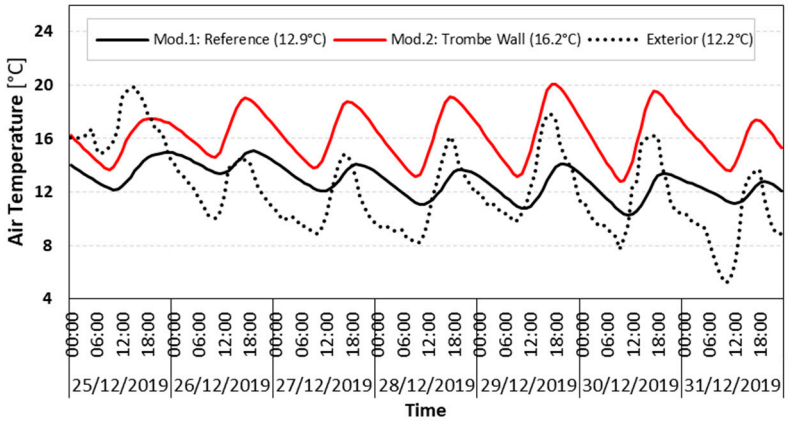

(**a**)

Figure 10. *Cont.*

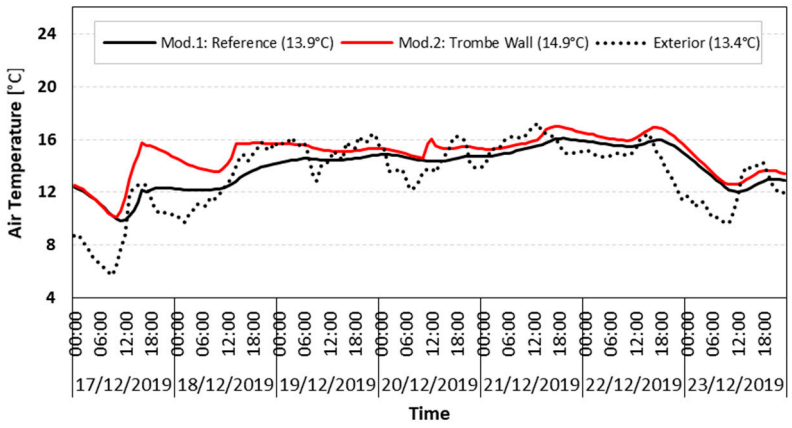

(**b**)

Figure 10. Recorded indoor air temperatures with and without a Trombe wall: (**a**) Winter sunny week; (**b**) Winter cloudy week.

When the sky was cloudy (Figure 10b), as expected, the daily temperature variation was very smothered, and the air temperature difference inside the modules became very reduced, which was only 1 °C higher for this week inside module 2. Comparing both weeks (sunny and cloudy), the average environment exterior air temperature was lower during the sunny week (Figure 10a) (12.2 °C) in comparison with the cloudy week (13.4 °C), which was 1.2 °C higher. This was due to the night cooling effect, which was much higher in a winter clear sky in comparison with a cloudy sky. Thus, this feature also demonstrated how important it was to control the night heat losses, mainly when the sky was clear, in order to optimize the thermal performance of the Trombe wall during the heating season.

3.1.2. Heating Energy Decrease

In this section, the heating energy decrease due to the existence of a Trombe Wall was predicted, making use of advanced numerical dynamic simulation models, as previously detailed in Section 2.2.2 and validated in Section 2.3. The hourly weather data was obtained from the EnergyPlus IWEC database [53] for Coimbra city (Portugal), and the computations were performed for all winter season (from 22nd of December until the 20th of March). The modeled air-conditioning heating system was a "split" type with no fresh air, having a coefficient of performance (COP) for heating mode equal to 2.35, with the adopted energy source the electricity from the grid.

To compare its relevance in the heating energy demand, two heating set-points were simulated, namely, 20 °C and 18 °C, respectively; the former and current thermal comfort temperatures considered for calculating residential heating energy needs in Portugal [54].

Moreover, two occupation schedules and use types were considered, namely, (1) an office space occupied from 08:00 to 18:00 during weekdays (Monday to Friday), and (2) a residential space occupied from 19:00 to 07:00 during all days. The predicted energy demand for heating (electricity) was displayed and analyzed as a total value (kWh) and as normalized values (kWh/m^2).

Residential Space Use (Heating during the Night)

The heating energy demand predicted for residential space use (night occupation) is displayed in Figure 11 for both LSF modules and two heating set-points. As expected, reducing the heating set-point (18 °C instead of 20 °C) allowed reducing also the heating energy consumption. This energy reduction was significant (Figure 11b), ranging from −33%, in the reference LSF module 1, to −40% in the Trombe wall LSF module 2.

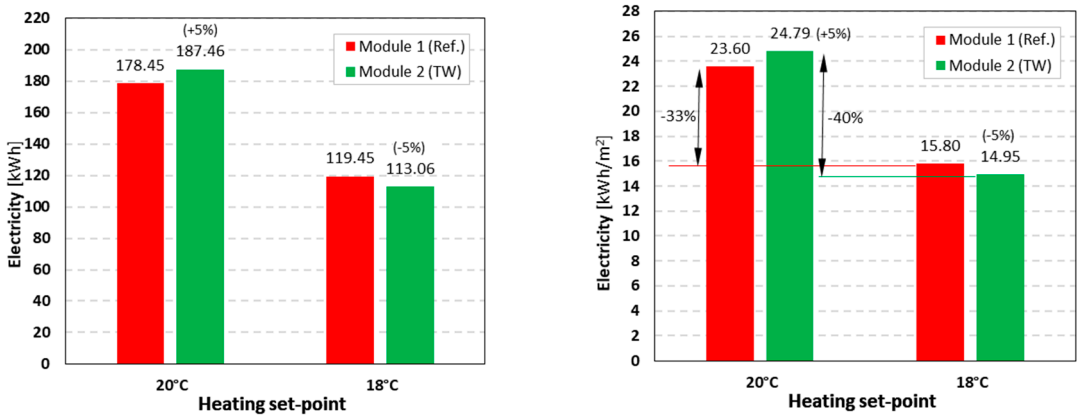

(**a**) (**b**)

Figure 11. Predicted heating energy consumption (electricity) during the winter season in Coimbra (Portugal), assuming residential space use, for two different set-points: (**a**) Total values; (**b**) Normalized values.

The heating energy consumption in module 2 was 5% lower than in module 1 for an 18 °C heating set-point, confirming the energy efficiency advantage of the Trombe wall (TW) in the second LSF module. However, when the heating set-point was higher (20 °C), the computed results showed a 5% increase in the heating energy for the TW module 2 (24.79 kWh/m^2) in comparison with the reference module 1 (23.60 kWh/m^2). This surprising feature was related to the increased heat losses during the night due to the existence of the TW in module 2, which were not enough to balance the solar heat gains during the daytime, and this assumption has been explained in detail in the following paragraphs.

The space heating energy demand, besides the efficiency of the air-conditioning system (assumed to be 2.35 for the heating mode in this work), depended on the heat balance (gains versus losses) for each module. When this heat balance was positive (e.g., during a sunny day due to significant solar heat gains), the indoor temperature arose. When this heat balance was negative (e.g., during the night due to the exterior temperature drop and absence of solar radiation), the indoor temperature decreased.

As measured and previously plotted in Figure 10a, the indoor temperature increase rate during the day was bigger in module 2 (red line) due to the higher solar heat gains provided by the Trombe wall. However, as also displayed in the same figure, during the night, the indoor temperature decrease rate was also bigger in the TW module 2, compared to the reference module 1 (black line), due to higher heat losses through the Trombe wall.

In fact, the thermal transmittance (*U*-value) of the TW device, due to air circulation between the glazed air-cavity and the interior of the module, was increased to the *U*-value of the glazing panel (2.552 W/(m^2·K), see Figure 3b). Comparing this *U*-value with the one provided by the LSF wall (0.326 W/(m^2·K), see Table 2), for the same area and temperature difference, the heat losses through the glazing panel of the TW were almost 7 times higher (+683%).

Obviously, when the indoor air temperature set-point was elevated from 18 °C up to 20 °C, the temperature difference between indoor and outdoor conditions also increased, leading also to an increase in the heat losses, which originated a higher space heating energy consumption to maintain the defined set-point indoor temperature. Once again, this feature reinforced the importance of mitigating heat losses through the TW, mainly during winter season night-time, for example, making use of a controllable night shutter device.

Office Space Use (Heating during the Day)

The heating energy demand simulation results, assuming an office space use, i.e., during the daytime, in both LSF modules, are displayed in Figure 12. Now, the energy efficiency benefits of the TW use were significantly higher in comparison with the residential daytime use (Figure 11). The heating

energy reduction ranged from −14%, for a 20 °C heating set-point, to −27% for an 18 °C set-point. This improved energy efficiency was because the heating schedule of the air-conditioning system matched the higher TW solar heating gains during the daytime. Consequently, the indoor temperature increased, and the heating energy use decreased for both heating set-points.

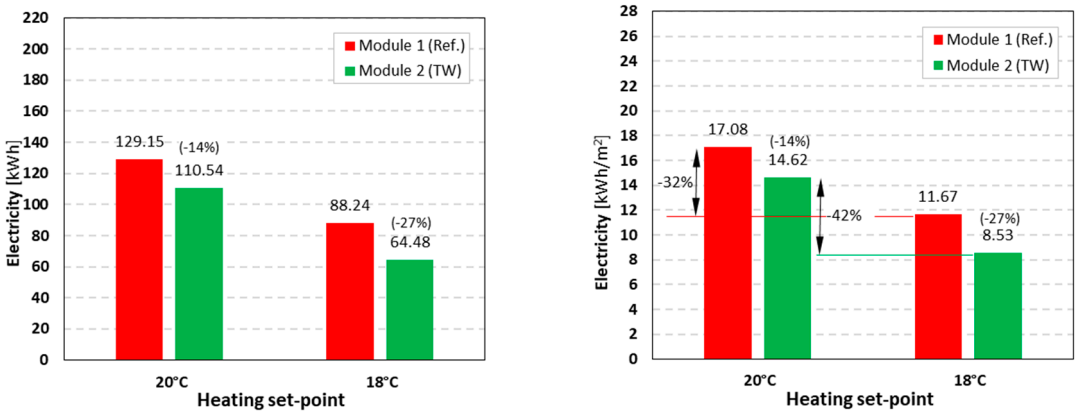

(**a**) (**b**)

Figure 12. Predicted heating energy consumption (electricity) during the winter season in Coimbra (Portugal), assuming office space use, for two different heating set-points: (**a**) Total values; (**b**) Normalized values.

Comparing the energy demand for both heating set-points, the energy reduction in percentages was similar to the previous ones, i.e., residential space use (Figure 11b), ranging from −32% up to −42% (Figure 12b), for reference LSF module 1 and TW module 2, respectively. However, in absolute values, this energy consumption reduction was smaller, i.e., −5.41 kWh/m^2 (office daytime use) instead of −7.80 kWh/m^2 (residential night-time use) for module 1, while for module 2, it was −6.09 kWh/m^2 instead of −9.84 kWh/m^2, for office and residential space use, respectively.

Jaber and Ajib [55] also performed hourly energy computer simulations to analyze the energy performance of a Trombe wall system for a typical Jordanian residential building (Mediterranean region). The studied house had a rectangular shape, having a floor area of about 154 m^2. The heavyweight façade walls had a very reduced thermal transmittance value, 0.133 W/(m^2·K), which corresponded to 41% of the LSF walls' *U*-value in the experimental modules, i.e., 0.326 W/(m^2·K) (see Table 2).

Their simulations were performed for a 20 °C heating set-point [55]. The predicted normalized heating energy consumption for the Jordanian building, without a Trombe wall, was 15.27 kWh/m^2, which was reduced to 12.09 kWh/m^2 (−21%), simulating a TW filling 18% of the south-oriented façade area (two bedrooms). They performed several simulations for different TW area ratios, ranging from 0% up to 50%, and based on the obtained results, they adjusted a polynomial curve (2nd order regression) to estimate the percentage of energy saving.

Making use of the previously mentioned estimation curve and applying the area ratio for the modular water TW evaluated in this paper, which was about 20%, the predicted energy saving would be around 22%. Not surprisingly, due to our reduced exterior walls insulation level, this energy-saving prediction was considerably higher than the ones obtained here for the 20 °C indoor set-point temperature.

3.2. Parametric Study

After analyzing the Trombe wall (TW) benefits in terms of indoor air temperature increase and heating energy decrease, in this section, a parametric study was conducted to assess the impact of the changes of some TW-related parameters on its thermal behavior. In this sensibility analysis, all the simulations were performed for the TW LSF module 2, having as reference for comparison the

DesignBuilder model, previously validated in Section 2.3.2, i.e., an unoccupied module. Notice that only one parameter was changed for each evaluated scenario, as displayed in Table 3. Four different parameters were evaluated: (1) Air cavity thickness; (2) Air vents dimensions; (3) Storage thickness; (4) Thermal storage material. For each parameter, two additional scenarios were assessed, besides the reference model scenario. Again, the hourly weather data for Coimbra (Portugal) was used [53], and a sunny winter week was chosen (23rd–29th January) for these simulations.

Table 3. Overview of evaluated parameters, models' identifications, and used values.

Parameter	Model	Value	
Air cavity thickness	Reference	10 cm	
	Scenario 1	20 cm	
	Scenario 2	30 cm	
Air vents dimensions	Reference	Lower	Upper
		50 × 5 cm	50 × 10 cm
	Scenario 3	50 × 8 cm	50 × 13 cm
	Scenario 4	50 × 11 cm	50 × 16 cm
Storage wall thickness	Reference	5 cm	
	Scenario 5	10 cm	
	Scenario 6	15 cm	
Thermal storage material	Reference	Water	
	Scenario 7	Concrete	
	Scenario 8	Basalt stone	

3.2.1. Air Cavity Thickness

The first TW parameter analyzed was the air cavity thickness between the storage wall and the glazed exterior frame. Three different air cavity thicknesses were evaluated: 10 cm (reference), 20 cm (scenario 1), and 30 cm (scenario 2), as illustrated in Figure 13. The increase in the air cavity thickness originated an indoor air temperature decrease. While the reference model had an average temperature of 18.2 °C, when the air cavity thickness was doubled (20 cm) and tripled (30 cm), the indoor temperature decreased to 0.9 °C and 1.2 °C, respectively. These results allowed to conclude that, for this TW configuration, the better thermal performance was achieved for the smaller air cavity (10 cm), which could be related to the lower air volume to be heated inside the air cavity and the higher buoyancy effect, promoting an increased upwards air convection and consequent higher heat flow through the upper vent to the interior of the module.

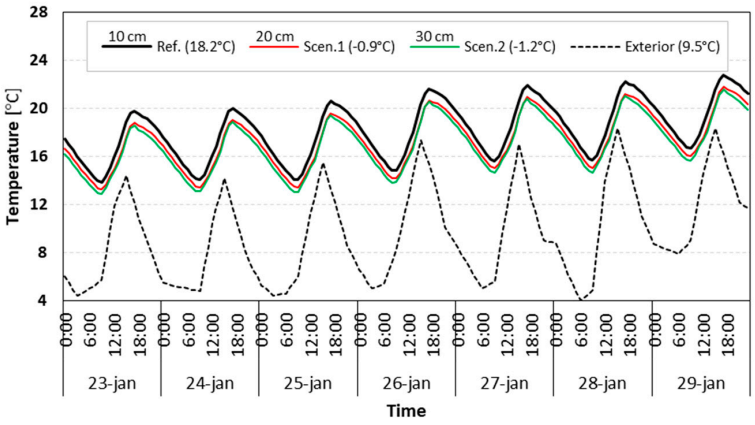

Figure 13. Influence of different air cavity thicknesses.

Hong et al. [56] performed a three-dimensional CFD thermal simulation of a Trombe wall with Venetian blind structure located in Hefei (China), assuming adiabatic surfaces for the air vents and internal wall. They compared several air cavity thicknesses, ranging from 8 cm up to 18 cm, with an increment of 2 cm. No significant thermal performance improvement was found for a thickness of the air cavity higher than 14 cm. Thus, they suggested a thickness equal to 14 cm.

3.2.2. Air Vents Dimensions

The second parameter analyzed was the dimension of the interior vents present on the storage wall to allow vertical air convection and airflow to/from the LSF module. The reference model had an upper vent with dimensions of 50 × 10 cm and a lower vent with 50 × 5 cm. Two additional scenarios were evaluated by modeling increased vents dimensions: 50 × 13 cm (upper) and 50 × 8 cm (lower) in scenario 3, and; 50 × 16 cm (upper) and 50 × 11 cm (lower) in scenario 4.

Figure 14 displays the obtained results, where a slightly indoor air temperature increase was visible with an increase in the dimensions of the air vents (+0.4 °C for scenario 3 and +0.5 °C for scenario 4). As expected, this indoor temperature increase was greater during the daytime, near noon, when the solar radiation was also higher. This better thermal performance could be justified by the increased natural air convection and airflow exchange between the TW air cavity and the interior of the module. Moreover, it could be deduced that forced air convection, making use of small fans, might improve, even more, the TW thermal performance.

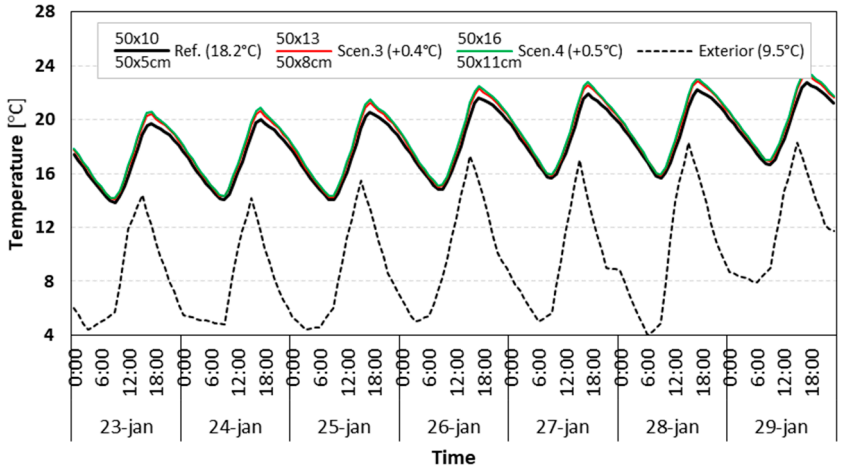

Figure 14. Influence of different dimensions of the air vents.

Hong et al. [56] also evaluated the influence of the inlet/outlet vent dimensions in the Trombe wall (2.00 m high × 1.00 m width) thermal performance. They assumed equal sized upper and lower vents and fixed their height to 10 cm. The vents width ranged from 20 cm up to 70 cm, with an increment of 10 cm. They found a slight decrease in the TW thermal performance for 70 cm width vents and suggested the use of vents with the following dimensions: 60 cm width × 10 cm height.

3.2.3. Storage Wall Thickness

The third parameter analyzed was the thickness of the water storage wall of the Trombe wall. The reference model had a 5 cm water storage wall composed of black painted steel, filled with water. Two additional scenarios with increased storage wall thickness were evaluated: 10 cm for scenario 5 and 15 cm for scenario 6.

Figure 15 exhibits the obtained results, where a decrease in indoor air temperature was visible in scenarios 5 (−0.7 °C) and 6 (−1.0 °C). This worst TW thermal performance could be justified by the larger volumes of water to be heated, inside the storage walls, by the same solar radiation and the consequent lower temperatures achieved.

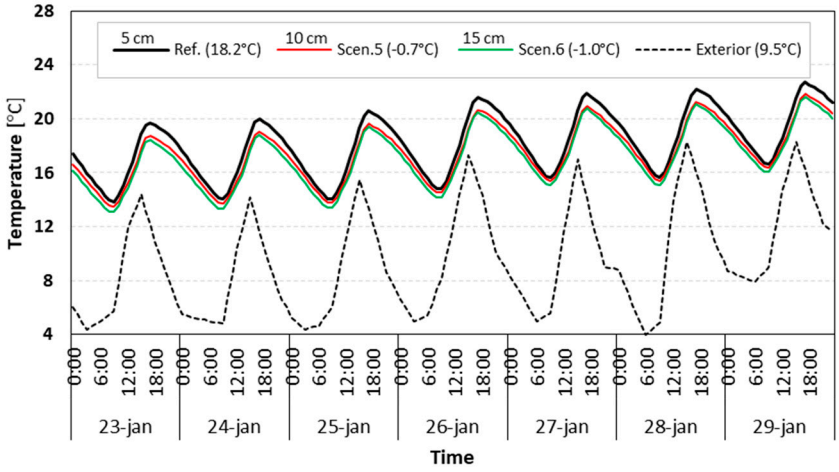

Figure 15. Influence of different storage wall thicknesses.

Briga-sá et al. [9] also evaluated the influence of the storage wall thickness (15 cm up to 40 cm), made of concrete, on ventilated and non-ventilated Trombe walls for the climate of Vila Real, a city located in the north of Portugal. Making use of a simplified calculation methodology prescribed by standard ISO13790:2008, they found that the heat gains were reduced when increasing the thickness for non-ventilated TWs, while for ventilated TWs, the heat gains increased.

3.2.4. Thermal Storage Material

The fourth and last parameter studied was the thermal storage material of the Trombe wall. As stated before, the reference TW thermal storage material was water. Two additional scenarios were simulated, making use of two other materials: concrete in scenario 7 and basalt stone in scenario 8. The thermal properties (thermal conductivity, specific heat, and density) of these three materials are displayed in Table 4. Regarding the optical properties, all these materials were modeled as being black painted, i.e., having solar and visible absorptances equal to 0.9.

Table 4. Thermal conductivity (λ), specific heat (c), and density (ρ) of thermal storage materials evaluated [37].

Material	λ ((m·K)/W)	c (J/(kg·K))	ρ (kg/m^3)
Water [1]	0.630	4190	990
Concrete	1.130	1000	2000
Basalt stone	3.490	840	2880

[1] For 40 °C temperature.

Figure 16 exhibits the obtained results, showing a slight decrease in the average indoor air temperature inside module 2 for the newly evaluated thermal storage materials: −0.4 °C for concrete (scenario 7) and −0.8 °C for basalt stone (scenario 8). Concrete storage material exhibited a higher temperature increase rate but also the higher temperature decrease rate during the cooling afternoon and night time, perhaps due to the significant lower specific heat (about four times smaller) and higher thermal conductivity (almost two times greater). The basalt stone temperature curve (scenario 8) exhibited a similar trend to the water temperature curve (Ref.), but with slightly lower indoor air temperature values (−0.8 °C).

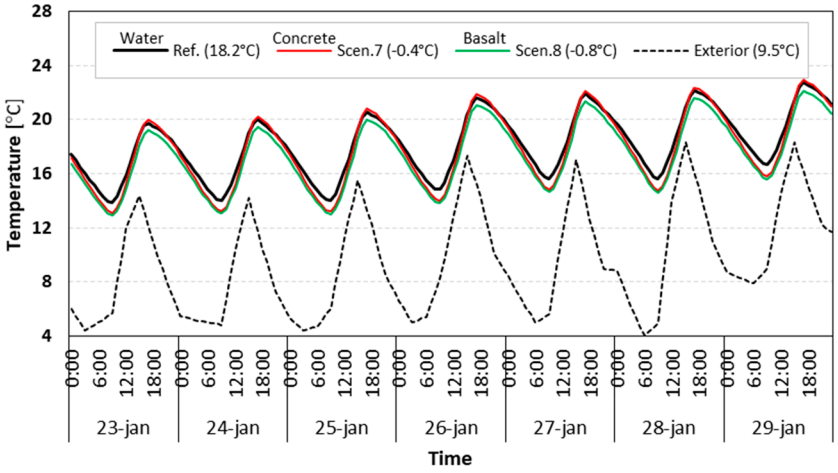

Figure 16. Influence of different thermal storage materials.

As stated by Saadatian et al. [7], "Because the specific heat of water (*c*) is higher than that of other types of building material, such as concrete, bricks, adobe, and stone, water stores more heat than the other materials. Similarly, because water convects, the transfer of heat to the interior space occurs faster than with classic Trombe walls.". Hu et al. pointed out another advantage of water as a thermal storage material: "Because the specific heat of water is higher than that of the building materials, the water's surface temperature does not rise as high as that of the masonry. Therefore, less heat is reflected back through the glazing." Nevertheless, Saadatian et al. [7], regarding water TWs, also stated that: "in harsh colder climates the glass layer should be insulated. Otherwise, the loss of heat from the warm wall to the outside would be significant.".

4. Conclusions

In this work, the influence of a passive modular water Trombe wall (TW) in the thermal behavior and energy efficiency of a lightweight steel frame (LSF) compartment was evaluated. Two real scale experimental identical LSF cubic modules, located in Coimbra (Portugal), exposed to natural exterior weather conditions, were used for in situ measurements. Module 1 was used as a reference, while the other one (module 2) was used to measure the influence of the TW, positioned in the south façade, on their thermal behavior by making a direct comparison between both modules. Additionally, these measurements allowed to calibrate and validate two numerical models (without and with a TW), with very good accuracy, i.e., having a root mean square error (RMSE) equal to 0.3 °C, for the reference model, and 0.5 °C for the TW model. These two validated models were used to perform advanced dynamic thermal simulations, making use of DesignBuilder software. Finally, these validated models allowed to predict the TW benefits in the heating energy consumption, as well as to perform a parametric study to evaluate the influence of four TW-related parameters on its thermal performance.

The first conclusion remark was that in this work, it was possible to evaluate the thermal behavior influence of a TW by in situ direct measurements and also performing advanced thermal dynamic simulations. The assessment was performed by quantifying the TW benefits (thermal and heating energy) and carrying out a thermal behavior parametric study. Several comparisons were performed, regarding (1) Sunny and cloudy winter week thermal behavior; (2) Office and residential space use heating energy; (3) Two heating set-points (20 °C and 18 °C); (4) Thickness of the TW air cavity; (5) Thickness of the thermal storage wall; (6) Dimensions of the interior upper/lower vents, and (7) Material of the thermal storage wall.

Regarding the obtained results for the TW benefits evaluation, the following main conclusions could be pointed out:

- In both sunny and cloudy winter weeks, the measured temperature was higher in module 2 (with a TW passive device). However, the warmer effect of the TW was much more effective during

the sunny week, increasing the average indoor air temperature significantly, i.e., +3.3 °C and +4.0 °C relative to the interior of module 1 (reference) and exterior environment temperatures, respectively.

- During the winter season, it was found that a TW was significantly more efficient for an office use schedule (during daytime), instead of a residential use schedule (during nigh-time). The heating energy consumption was reduced from 14.95 kWh/m^2, for residential space, down to 8.53 kWh/m^2 for office space (−43%), for an 18 °C indoor comfort temperature.
- A smaller heating set-point (18 °C instead of 20 °C) allowed to significantly reduce the heating energy consumption with and without a TW device, more than 40% and 32% reductions, respectively.
- A 27% reduction in heating energy due to TW device for an office 18 °C set-point was found, and this energy reduction was smaller (−14%) for the heating 20 °C set-point.

For residential use, the TW energy benefits were very reduced (only 5% decrease for 18 °C set-point), and there was even a heating energy consumption increase (+5%) when the set-point was 20 °C, due to nocturnal heat losses through the TW device.

Regarding the TW device parametric study, the main conclusions could be summarized as follows:

- An increase in the original TW air cavity thickness (10 cm) did not show any thermal performance improvement, and a decrease in the average indoor air temperature was found (−0.9 °C and −1.2 °C).
- Increasing the dimensions of the interior upper/lower TW vents (50 × 10 cm / 50 × 5 cm) allowed to slightly increase their thermal performance (+0.4 °C and +0.5 °C).
- An increase in the original thermal storage wall thickness (5 cm) did not show any thermal performance improvement, and a decrease in the average indoor air temperature was obtained (−0.7 °C and −1.0 °C).
- Changing the material of the storage wall (water) reduced the thermal performance of the TW device, originating a decrease in the average indoor air temperature (−0.4 °C and −0.8 °C).

In short, a TW device could, in fact, significantly improve the thermal behavior of an LSF compartment and reduce heating energy consumption during winter in a Csb Köppen–Geiger [47] Mediterranean climate. However, there were many factors that could influence the TW thermal performance, with adequate design and control to mitigate nocturnal heat losses very important. Otherwise, their thermal performance and energy efficiency improvement could be very insignificant and even decreased.

As most of the research studies, this work also had some limitations, including the assessment of only one climate/location, only one TW orientation (south exposed), only one isolated small compartment (not an entire building) without any window, only one construction system (LSF), only the heating mode during the winter season was evaluated (not an entire year), etc. Thus, in real buildings, thermal behavior and energy performance are much more complex, depending on many more factors. Nevertheless, the obtained results and conclusions could be very useful to identify the main benefits and possible drawbacks of a solar passive TW device in an LSF compartment, as well as to enhance the importance of the indoor set-point temperature and the occupation schedule of the compartment.

Author Contributions: All the authors participated equally in this work. All authors have read and agreed to the published version of the manuscript.

Funding: This research work was supported by ISISE (Institute for Sustainability and Innovation in Structural Engineering) and funded by FEDER funds through the Competitivity Factors Operational Programme—COMPETE and by national funds through FCT—Foundation for Science and Technology within the scope of the project POCI-01-0145-FEDER-032061.

Cofinanciado por: POCI-01-0145-FEDER-032061

Acknowledgments: The Trombe wall prototype was manufactured by CoolHaven company, and the experimental modules were built with the support of the following companies: Urbimagem; Fachaimper; CoolHaven; Forbo flooring systems; Weber (Saint-Gobain); Termolan; Bifase; Sociveda; Falper, and FibroPlac.

Conflicts of Interest: The authors declare no conflict of interest.

Acronyms

2D	Two-Dimensional
CFD	Computational Fluid Dynamics
DEC	Department of Civil Engineering
DEM	Department of Mechanical Engineering
EPBD	Energy Performance of Buildings Directive
EPS	Expanded Polystyrene
ETICS	External Thermal Insulation Composite System
EU	European Union
FEM	Finite Element Method
GPB	Gypsum Plasterboard
GPS	Global Positioning System
GWTW	Glass-Water Trombe Wall
HFM	Heat Flow Meter
ISO	International Standards Organization
LSF	Lightweight Steel Frame
MW	Mineral Wool
N	North
nZEB	nearly Zero-Energy Buildings
OSB	Oriented Strand Board
PhD	Doctor of Philosophy
PVC	Polyvinyl Chloride
RMSE	Root Mean Square Error
S	South
SHGC	Solar Heat Gain Coefficient
TC	Thermocouple
TTW	Traditional Trombe Wall
TW	Trombe Wall
W	West
WTW	Water Trombe Wall
XPS	Extruded Polystyrene

References

1. European Union. Directive (EU) 2018/844 of the European Parliament and of the Council of 30 May 2018 amending Directive 2010/31/EU on the energy performance of buildings and Directive 2012/27/EU on energy efficiency. In *Official Journal of the European Union*; European Parliament: Luxembourg, 2018; pp. 75–91.
2. European Union. Directive 2010/31/EU of the European Parliament and of the Council of 19 May 2010 on the energy performance of buildings. In *Official Journal of the European Union*; European Parliament: Luxembourg, 2010; pp. 13–35.
3. Brandão De Vasconcelos, A.; Pinheiro, M.D.; Manso, A.; Cabaço, A. EPBD cost-optimal methodology: Application to the thermal rehabilitation of the building envelope of a Portuguese residential reference building. *Energy Build.* **2016**, *111*, 12–25. [CrossRef]

4. Attia, S.; Eleftheriou, P.C.; Xeni, F.; Rodolphe, M.; Ménézo, C.; Kostopoulos, A.; Betsi, M.; Kalaitzoglou, I.; Pagliano, L.; Cellura, M.; et al. Overview and future challenges of nearly zero energy buildings (nZEB) design in Southern Europe. *Energy Build.* **2017**, *155*, 439–458. [CrossRef]
5. D'Agostino, D.; Parker, D. A framework for the cost-optimal design of nearly zero energy buildings (NZEBs) in representative climates across Europe. *Energy* **2018**, *149*, 814–829. [CrossRef]
6. Hu, Z.; He, W.; Ji, J.; Zhang, S. A review on the application of Trombe wall system in buildings. *Renew. Sustain. Energy Rev.* **2017**, *70*, 976–987. [CrossRef]
7. Saadatian, O.; Sopian, K.; Lim, C.H.; Asim, N.; Sulaiman, M.Y. Trombe walls: A review of opportunities and challenges in research and development. *Renew. Sustain. Energy Rev.* **2012**, *16*, 6340–6351. [CrossRef]
8. Wang, D. Classification, experimental assessment, modeling methods and evaluation metrics of Trombe walls. *Renew. Sustain. Energy Rev.* **2020**, *124*, 109772. [CrossRef]
9. Briga-Sá, A.; Martins, A.; Boaventura-Cunha, J.; Lanzinha, J.C.; Paiva, A. Energy performance of Trombe walls: Adaptation of ISO 13790:2008(E) to the Portuguese reality. *Energy Build.* **2014**, *74*, 111–119. [CrossRef]
10. Li, W.; Chen, W. Numerical analysis on the thermal performance of a novel PCM-encapsulated porous heat storage Trombe-wall system. *Sol. Energy* **2019**, *188*, 706–719. [CrossRef]
11. Lin, Y.; Ji, J.; Zhou, F.; Ma, Y.; Luo, K.; Lu, X. Experimental and numerical study on the performance of a built-middle PV Trombe wall system. *Energy Build.* **2019**, *200*, 47–57. [CrossRef]
12. Zhou, L.; Huo, J.; Zhou, T.; Jin, S. Investigation on the thermal performance of a composite Trombe wall under steady state condition. *Energy Build.* **2020**, *214*, 109815. [CrossRef]
13. Hu, Z.; Zhang, S.; Hou, J.; He, W.; Liu, X.; Yu, C.; Zhu, J. An experimental and numerical analysis of a novel water blind-Trombe wall system. *Energy Convers. Manag.* **2020**, *205*, 112380. [CrossRef]
14. Hong, X.; Leung, M.K.H.; He, W. Effective use of venetian blind in Trombe wall for solar space conditioning control. *Appl. Energy* **2019**, *250*, 452–460. [CrossRef]
15. Abbassi, F.; Dimassi, N.; Dehmani, L. Energetic study of a Trombe wall system under different Tunisian building configurations. *Energy Build.* **2014**, *80*, 302–308. [CrossRef]
16. Santos, P.; Simões da Silva, L.; Ungureanu, V. *Energy Efficiency of Light-Weight Steel-Framed Buildings*, 1st ed.; European Convention for Constructional Steelwork (ECCS), Technical Committee 14—Sustainability & Eco-Efficiency of Steel Construction: Mem Martins, Portugal, 2012; ISBN 978-92-9147-105-8.
17. Santos, P.; Martins, C.; Simões Da Silva, L. Thermal performance of lightweight steel-framed construction systems. *Metall. Res. Technol.* **2014**, *111*, 329–338. [CrossRef]
18. Murtinho, V.; Ferreira, H.; Antonio, C.; Simoes da Silva, L.; Gervasio, H.; Santos, P. Architectural concept for multi-storey apartment building with light steel framing. *Steel Constr.* **2010**, *3*, 163–168. [CrossRef]
19. Santos, P. Chapter 3—Energy Efficiency of Lightweight Steel-Framed Buildings. In *Energy Efficient Buildings*; Eng Hwa, Y., Ed.; InTech: London, UK, 2017; pp. 35–60.
20. Gervásio, H.; Santos, P.; Martins, R.; Simões da Silva, L. A macro-component approach for the assessment of building sustainability in early stages of design. *Build. Environ.* **2014**, *72*, 256–270. [CrossRef]
21. Gervásio, H.; Santos, P.; Simões da Silva, L.; Lopes, A.M.G. Influence of thermal insulation on the energy balance for cold-formed buildings. *Adv. Steel Constr.* **2010**, *6*, 742–766.
22. Santos, P.; Martins, R.; Gervásio, H.; Silva, L.S. Assessment of building operational energy at early stages of design—A monthly quasi-steady-state approach. *Energy Build.* **2014**, *79*, 58–73. [CrossRef]
23. Martins, C.; Santos, P.; Simoes da Silva, L. Lightweight steel-framed thermal bridges mitigation strategies: A parametric study. *J. Build. Phys.* **2016**, *39*, 342–372. [CrossRef]
24. Roque, E.; Santos, P. The Effectiveness of Thermal Insulation in Lightweight Steel-Framed Walls with Respect to Its Position. *Buildings* **2017**, *7*, 13. [CrossRef]
25. Soares, N.; Gaspar, A.R.; Santos, P.; Costa, J.J. Multi-dimensional optimization of the incorporation of PCM-drywalls in lightweight steel-framed residential buildings in different climates. *Energy Build.* **2014**, *70*, 411–421. [CrossRef]
26. Özdenefe, M.; Atikol, U.; Rezaei, M. Trombe wall size-determination based on economic and thermal comfort viability. *Sol. Energy* **2018**, *174*, 359–372. [CrossRef]
27. Duan, S.; Jing, C.; Zhao, Z. Energy and exergy analysis of different Trombe walls. *Energy Build.* **2016**, *126*, 517–523. [CrossRef]

28. Soares, N.; Santos, P.; Gervásio, H.; Costa, J.J.; Simões da Silva, L. Energy efficiency and thermal performance of lightweight steel-framed (LSF) construction: A. review. *Renew. Sustain. Energy Rev.* **2017**, *78*, 194–209. [CrossRef]
29. LSF System B(A)a, by 'Balthazar Aroso Arquitectos, Lda', Manufactured by Urbimagem—Sistemas de Arquitectura e Construção, Lda, 2019. Available online: www.urbimagem.com/en/empresa/ (accessed on 10 March 2019).
30. Norbord. Technical Brochure—OSB3 Zero. 2019. Available online: www.norbord.co.uk/our-products/sterlingosb-zero/sterlingosb-zero-osb3/ (accessed on 10 March 2020).
31. Termolan. Technical Brochure—PA30 Mineral Wool, 2019. 2019. Available online: http://termolan.pt/wp-content/uploads/2018/06/pa30-pt.pdf (accessed on 10 March 2020).
32. Weber(Saint-Gobain). Technical Brochure—EPS100, Weber.Therm Classic, 2019. Available online: www.pt.weber/files/pt/2019-04/FichaTecnica_sistema_webertherm_classic.pdf (accessed on 10 March 2020).
33. Danopren. Technical Brochure—XPS TL-P 50, 2019. Available online: https://portal.danosa.com/danosa/CMSServlet?node=483103&lng=4&site=3 (accessed on 10 March 2020).
34. TEC. Technical Brochure—XPS RoofTEC SL/FloorTEC 300, 2019. Available online: www.sotecnisol.pt/resources/777f40511b178afb7f9e2c1a7a9e55af/fichas_tecnicas/dop_rooftec.floortec_50_2016_por.pdf (accessed on 10 March 2020).
35. Danopol. Technical Brochure—Water-Proofing PVC Membrane: HSF 1.5 Light Grey, 2019. Available online: https://portal.danosa.com/danosa/CMSServlet?node=210302&lng=4&site=3 (accessed on 10 March 2020).
36. Rosa, N.C.F. Study of structural and thermal performance of lightweight steel framing (LSF) modular construction. Ph.D. Thesis, University of Coimbra, Coimbra, Portugal, 2018.
37. DesignBuilder. DesignBuilder Software Version 5.5.0.012 and Materials Database, 2018. Available online: https://designbuilder.co.uk/ (accessed on 14 February 2019).
38. Santos, C.; Matias, L. *ITE50—Coeficientes de Transmissão Térmica de Elementos da Envolvente dos Edifícios (in Portuguese)*; LNEC—Laboratório Nacional de Engenharia Civil: Lisboa, Portugal, 2006.
39. Sarlon. Technical Brochure—Vinyl Acoustic Flooring: Sarlon Traffic 19dB, 2019. Available online: www.forbo.com/flooring/en-aa/products/acoustic-flooring/sarlon-trafic-19-db/blbfkp (accessed on 10 March 2020).
40. Vicaima. Technical Brochure—Wooden Door: Portaro-SBD-EI30. 2019. Available online: www.vicaima.com/files/files/Vicaima-FT-Portaro-SBD-EI30.pdf (accessed on 10 March 2020).
41. ISO 6946. *Building Components and Building Elements—Thermal Resistance and Thermal Transmittance—Calculation Methods*; International Organization for Standardization: Geneva, Switzerland, 2017.
42. THERM. Software Version 7.6.1. Lawrence Berkeley National Laboratory, United States Department of Energy, 2017. Available online: https://windows.lbl.gov/software/therm (accessed on 14 February 2019).
43. DEM Weather Station. ADAI@DEM.UC Weather Station Located in the Dep. of Mechanical Engineering, University of Coimbra, Portugal, 2020. Available online: www.wunderground.com/dashboard/pws/ICOIMBRA14 (accessed on 15 February 2020).
44. CoolHaven. CoolHaven—Modular Constructions, 2020. Available online: www.cool-haven.com (accessed on 15 February 2020).
45. Davis Instruments. Wireless Vantage Pro2 Plus Automatic Weather Station, Including UV and Solar Radiation Sensors, from Davis Instruments, 2019. Available online: www.davisinstruments.com/product/wireless-vantage-pro2-plus-including-uv-solar-radiation-sensors/ (accessed on 15 February 2019).
46. Delta-T Devices. Sunshine Sensor BF5 (pyranometer), from Delta-T Devices, 2019. Available online: www.delta-t.co.uk/product/bf5/ (accessed on 15 February 2019).
47. Kottek, M.; Grieser, J.; Beck, C.; Rudolf, B.; Rubel, F. World Map of the Köppen-Geiger climate classification updated. *Meteorol. Zeitschrift* **2006**, *15*, 259–263. [CrossRef]
48. Tinytag. Tinytag Ultra 2—TGU-4500, TGU-4500—Indoor Temperature and Relative Humidity Data Logger with Built-in Sensors, 2019. Available online: https://www.geminidataloggers.com/data-loggers/tinytag-ultra-2/tgu-4500 (accessed on 15 February 2019).
49. Santos, P.; Gonçalves, M.; Martins, C.; Soares, N.; Costa, J.J. Thermal Transmittance of Lightweight Steel Framed Walls: Experimental Versus Numerical and Analytical Approaches. *J. Build. Eng.* **2019**, *25*, 100776. [CrossRef]
50. Santos, P.; Lemes, G.; Mateus, D. Analytical Methods to Estimate the Thermal Transmittance of LSF Walls: Calculation Procedures Review and Accuracy Comparison. *Energies* **2020**, *13*, 840. [CrossRef]

51. Santos, P.; Lemes, G.; Mateus, D. Thermal Transmittance of Internal Partition and External Facade LSF Walls: A Parametric Study. *Energies* **2019**, *12*, 2671. [CrossRef]
52. Tyre4BuildIns. Research Project Tyre4BuildIns—'Recycled Tyre Rubber Resin-Bonded for Building Insulation Systems towards Energy Efficiency', Funded by FEDER European and FCT National Funds. Reference: POCI-01-0145-FEDER-032061. University of Coimbra, Portugal, 2020. Available online: www.tyre4buildins.dec.uc.pt (accessed on 15 January 2020).
53. PRT_Coimbra.085490_IWEC. International Weather for Energy Calculation (IWEC), Weather Data for Coimbra (WMO Station 085490), EnergyPlus Weather Database, 2009. Available online: https://energyplus.net/weather-location/europe_wmo_region_6/PRT//PRT_Coimbra.085490_IWEC (accessed on 15 February 2019).
54. REH. *Portuguese Regulation for Energy Performance of Residential Buildings (in Portuguese), Approved by Decree-Law n. 118/2013 of 20 August*; N. 159; Diário da República – I série (in Portuguese): Lisboa, Portugal, 2013; pp. 4988–5005.
55. Jaber, S.; Ajib, S. Optimum design of Trombe wall system in mediterranean region. *Sol. Energy* **2011**, *85*, 1891–1898. [CrossRef]
56. Hong, X.; He, W.; Hu, Z.; Wang, C.; Ji, J. Three-dimensional simulation on the thermal performance of a novel Trombe wall with venetian blind structure. *Energy Build.* **2015**, *89*, 32–38. [CrossRef]